Preprint: *Granular Matter* (to appear 2007)

Effects of gravity on cohesive behavior of fine powders: implications for processing Lunar regolith

Otis .R. Walton

Grainflow Dynamics Inc., Livermore, CA 94550

Tel: 925-447-2276

Fax: 925-449-9111

walton@grainflow.com

www.grainflow.com

C. Pamela De Moor

Alza Corp., Palo Alto, CA

Tel: 650-564-5921

Fax: 650-564-2484

pdemoor@alzus.jnj.com

Karam S. Gill

Grainflow Dynamics Inc.

Tel 310-699-5973

karamgill@hotmail.com

Abstract It is well known that powders become more 'cohesive' as their mean particulate size decreases. This phenomenon is evidenced by such characteristics as poor flowability, clumping, avalanching, difficulty in fluidizing, and formation of quasi-stable, low-density configurations that are easily compacted. Gravity is often the primary driving force for powder movement in common powder processing and transfer operations. Because of this, gravity plays a role in how the flow behavior of powders is typically characterized. As a result, the 'cohesiveness' of a powder varies with gravity-level, with a powder appearing more 'cohesive' as the effective gravity level is decreased. In this work the change in powder flow behavior with *g*-level is clearly demonstrated by observing the transition from avalanching flow to smooth flow as the effective *g*-level is increased, and vice versa. Experiments with micron-scale pharmaceutical powders in a centrifuging, rotating-drum micro-avalancher, covering *g*-levels from 12.5 to 1200 (a factor of 100 variation in *g*-level) clearly demonstrate the changes from clumping (with no flow), to avalanching flow, to free-flowing behavior as the effective *g*-level is increased. A mere factor of four change in effective *g*-level (from $25g_o$ to $100g_o$) was sufficient to show a significant change from avalanching behavior to free flowing behavior for more than one powder tested. Extrapolation of this same behavior to gravity levels below our terrestrial level (such as to the $1/6 - g_o$ conditions on the moon) would indicate that Lunar regolith will exhibit more 'cohesive' behavior in

processing, transfer and handling equipment than the same powder would exhibit terrestrially. Thus, Lunar in-situ resource utilization (ISRU) processes may need to use larger size openings, steeper slopes or non-gravity driving forces in processing, transfer and handling equipment than would be used for comparable powders and processes on earth.

Keywords: *cohesive-powder rotating-drum avalanche angle-of-repose centrifuge lunar-regolith high-gravity*

1 Introduction and Background

Most of the lunar surface is covered with regolith, a mixture of fine dust and rocky debris produced by meteor impacts and varying in thickness from about 5 *m* on mare surfaces to about 10 *m* on highland surfaces. The bulk of the regolith is a fine gray soil with a bulk density of about 1.5 g/cm^3, but it also contains breccia and rock fragments from the local bed rock [1, 2, 3]. The large number of very fine particles increases the surface area per unit mass, and thus the surface energy per unit mass available for cohesive forces to act in the bulk material. Also, the absence of air and water has allowed the fines to remain in the regolith as a greater percentage of the mass than would be typical of terrestrial geologic deposits. Although the solids fraction of in-situ Lunar regolith is relatively high (often 50% solids or greater) it is expected that, if this material were disturbed (as in ISRU operations) it could form low-density, stable configurations ('fluff') typical of any fine cohesive powder under 'sifted' conditions. Taken to extremes, very fine cohesive powders can exhibit bulk solids fractions that are as low as 10% even under terrestrial gravity conditions. An example of such a material, with which many readers might be familiar, is new fallen *powder snow*, that occurs when the temperature is well below freezing. This bulk material is comprised of small ice crystals (of density 1g/cc) but it exists as a very low density bulk material, which is quite compressible. The low-density wind-blown Martian dust that the rover Opportunity was stuck in for over a month, in May 2005, may be an example of a material with properties not unlike fresh powder snow.

[A comment on notation, throughout this paper g_o is meant to be the acceleration of gravity on the earth's surface, e.g. $g_o \sim 9.8 m/s^2$; while *g*-level, generally indicates a multiple of g_o. In some figures and elsewhere, however, the subscript, $_o$, is omitted primarily because many figures were electronically imported as images and could not be edited readily.]

Cohesiveness, Flowability and Compaction Behavior:

Despite there being a variety of measurement methods available [4], there is no uniformly accepted definition for the *cohesiveness* or *cohesivity* of a powder, nor for powder *flowability* [5] In making such a statement we are distinguishing between the *cohesive-strength* of a material (for which there are standard geotechnical measurement methods) and the *cohesive-behavior* of a powder, which is a qualitative description of how a powder flows in a particular size piece of equipment and with a particular level of driving force. It is generally recognized that the flow

behavior of a powder is related to its *shear-strength*, a property which is both a state and history-dependent variable (as is a powder's *cohesive-strength*). In soil mechanics the *cohesive-strength* of a bulk material is well defined and it can be measured with standard geotechnical laboratory methods such as a triaxial test. There are a variety of other methods to measure the *shear strength* of a powder, utilizing direct shear, such as the Jenike [6], Schulze [7], or Pschl [8] shear cells which can measure the *yield loci* or *failure envelope* of a powder and, in some cases, how it varies with precompaction, or previous stress-strain history. The *cohesive-strength* of a weakly cohesive powder can also be measured directly (e.g. the Sevilla powder tester [9]). Index tests also exist to rank the *flowability* of powders [10, 11].

The *compressibility* of a powder is often associated with its cohesiveness and has formed the basis for a variety of index tests for ranking the *cohesiveness* or *cohesivity* powders. Cohesive powders existing in low-density 'sifted' states, are quite compressible, and can easily be compacted to higher densities by external loads, or by handling or jarring their containers. The pharmaceutical industry routinely deals with fine cohesive powders and often characterizes how cohesive a powder is by its Hausner ratio, that is, the ratio of the density after being 'tapped' repeatedly (up to thousands of times in a controlled tapped-density test) to initial sifted density [12, 13]. Such tapped-density tests serve as index tests to classify the cohesiveness of powders. For a more quantitative measure of cohesive powder compaction, one can examine the stress *vs.* density behavior under controlled uniaxial or isotropic compression. The authors (especially CPD) have found low-stress-level uniaxial compaction of cohesive powders to be a reproducible and reliable indicator of the cohesive nature of a powder. Figure 1 compares the solids fraction as a function of axial stress during uniaxial compaction of fine, cohesive powders comprised of nearly spherical raffinose particles made by spray drying an aqueous solution with different mass fractions of raffinose, ranging from 0.05% to 25%, in a bench-scale (Büchi) spray dryer [14,15], and similar compaction (oedometer) data for Russian lunar regolith samples Luna 16 and 20 [1]. The Luna samples are comprised of typical non-spherical, angular, regolith with a median size of 60 μm, or so, and perhaps a somewhat higher fraction of agglutinates than most Apollo samples (The median size of the Luna sample particles is not stated in the Lunar Sourcebook [1]; however, typical Apollo, sub-millimeter regolith samples had median sizes on the order of 50 – 70 μm). The Luna samples were certainly not as fine nor as cohesive as the raffinose powders used in the tests shown in Figure 1; however, they did exhibit an unusually low initial solids fraction – a feature often associated with very cohesive powders (although there is some speculation that the low solids fraction of the Luna samples is due to their unusually high agglutinate content [M. Nakagawa, Colorado School of Mines, personal communication, 2006]). The median particle size for the raffinose powders shown in Figure 1 ranged from approximately 0.8μm to ~4μm. As seen in this figure, the initial solids fraction of the raffinose powder ranged from 10% to 25%, and they each compacted by a factor of from 2.5 to 4 in going from 0.01*Bar* to 1*Bar* pressure. The particles in the raffinose samples of Figure 1 are particularly cohesive, and they also have relatively large contact-spot areas when they 'touch' neighboring particles because they are nearly spherical. The specific surface area, in meters squared per gram, for each of the powders in Figure 1, is shown in

parentheses next to the individual curve. A higher specific surface area is usually associated with finer, more cohesive powders.

Figure 2 shows an SEM of particles from one of the raffinose powder samples [15]. Lunar or Martian soil or crushed rocks are not expected to be as cohesive as the raffinose powders of Figures 1 and 2; however, experience gained with centrifuging rotating drums and under various gravity levels on NASA's KC-135 indicate that powders tend to exhibit more cohesive behavior when the driving force for flow (*i.e.*, gravity) is small. Conversely, as shown below, they can behave more like cohesionless powders as the effective gravity level is increased.

Flow in Rotating Drums:

Rotating drums are a common configuration for many mineral or powder processing operations. They also form the basis for various powder flow characterization instruments. In this paper we use flow in a rotating drum as a convenient method of demonstrating the changes in powder flow behavior as the effective gravity-level changes.

Flow of cohesionless granular materials in partially filled rotating drums exhibit a range of behaviors depending on the rotation rate of the drum [16], including:

- Periodic avalanches at low rotation rates
- A nearly-linear top surface in the 'dynamic angle of repose' range
- Bi-linear or S-shaped top surface at higher rotation rates

(Cohesive powders, on the other hand, exhibit large build-up and collapse of steep structures in the upper half of the top surface layer, with a chaotic time dependence – these will be discussed in more detail later in this paper).

The nearly-linear dynamic-angle-of-repose regime for cohesionless powders occurs when the duration of an individual avalanche is close to the period between avalanches, so that the motion becomes nearly continuous. Thus, the rotation rates at which this flow regime exists depend not only on the gravity driving force, but also, on the physical size of the drum and the characteristics of the specific granular material. In order to ensure that the same flow-mode would be observed at different *g*-levels in a rotating drum apparatus constructed for this research, a series of discrete element method (DEM) simulations were performed [17], using cohesionless, frictional, inelastic spheres [18, 19]. Figure 3 shows the variation of the dynamic angle of repose obtained in those simulations over a factor of two variation in rotation rate, for a 0.136*m* diameter drum, partially filled with 3.78*mm* diameter spheres (of mass $4.086 \times 10^{-5} kg$). The 3-D simulation cell was approximately 5 particle-diameters thick (along the drum axis) and had periodic boundaries on the 'ends'. The interparticle coefficient of friction in these simulations was set to 0.4 and the coefficient of restitution was 0.85, using the bi-linear, Walton-Braun partially latching spring model [20]. The simulation results were consistent with known qualitative behavior for cohesionless granular materials in slowly rotated drums [16, 21]. Moreover, it was observed that the angle of repose exhibited by the simulated spheres varied almost linearly with the rotation rate over a range of approximately a factor of two in rotation rate (e.g., as demonstrated by the hand-

drawn straight line within the error-bars of the simulation results shown in Figure 3). This is consistent with measured behavior in rotating drums [22]. At higher rotation rates inertial overshoot occurred at the upper end, and the top surface was no longer nearly-linear. At lower rotation rates, regular periodic avalanching occurred. When the rotation-rate was held fixed and the *g*-level increased by an order of magnitude, the simulated material exhibited periodic avalanching behavior. Conversely, when the *g*-level was decreased by an order of magnitude at constant rotation rate, inertial overshoot occurred and the top surface did not remain linear. However, when the *rotation rate was scaled with the square root of the g-level*, the simulations produced *the same apparent dynamic-angle-of-repose at all g-levels from 1-g_o to 1000-g_o* (within the uncertainty shown by the error-bars on Figure 3). This was a crucial design scaling relation needed before constructing an angle-of-repose test apparatus, designed to produce the same mode of flow at different *g*-levels, with a minimum of effort, in a single test series. Although it was recognized that the mode of flow is also dependent on the physical size of the apparatus, the size-scaling relation was not determined with additional simulations, since the physical tests were to be conducted with a fixed cell size, and the actual rotation rate that would produce the desired flow-mode could be readily determined empirically with the test apparatus, once it was constructed.

Other flow-modes were also examined both in simulations and experimentally, although they will not be discussed in great detail in this paper. For example, at very high rotation rates (e.g., just below a rate where the centrifugal acceleration would keep the material on the outer wall at the top) the inertial overshoot can cause the material to cascade like a cresting wave, impacting the material near the bottom of the drum with relatively high intensity. This is the mode of flow in a typical media-mill or ball-mill for grinding fine powders. Figures 4(a) and 4(b) show DEM simulations of cohesionless spheres in a rotating drum at 1-g_o with a ratio of centrifugal acceleration to *g*-level of approximately one [23]. Figure 4(c) shows a snapshot of weakly-cohesive 4μm BCR-Limestone powder [30] in a 3/8" diameter planetary mill configuration with the main centrifuging acceleration, A_c, at 330g_o and the rotation rate of the small drum such that the centrifugal acceleration at its periphery, a_c, is 0.8 times the main centrifuging acceleration, A_c [24]. Although the scale and rotation rates are different in the simulation and the test, the cascading or cresting mode of motion is similar. Figure 5 is a schematic of one embodiment of a planetary-mill configuration (with two small rotating drums) illustrating the relationships between the various rotation rates, radii, and centrifugal accelerations.

Klein and White [25] conducted experiments on rotating drum flows at various *g*-levels from 0.1 to 1.8 times earth's nominal $g_o = 9.8m/s^2$ utilizing NASA's low-gravity KC-135 aircraft. Their apparatus consisted of a 0.22*m*-diameter, by 0.1*m*-long belt-driven drum. They tested both glass beads (mean diam = 1.35*mm*) and Monterey sand (mean diam = 0.4*mm*), with quantities that filled less than 10% of the volume of the drum. The glass beads exhibited the greatest change in angle of repose with *g*-level and those tests were reexamined as part of this work. Klein & White used a non-dimensionalizing factor to analyze their results that was equivalent to assuming that, at constant *g*-level, the angle of repose was proportional to the rotation-rate to the ¾ power (*i.e.*, $\theta_r \propto \omega^{3/4}$). This functional form was selected on the basis of a dimensional analysis which included the viscosity and density of the interstitial fluid (air). As part of the current investigation,

Klein and White's experiments, both at 1-g_o and in flight at various g-levels, were re-analyzed to see if they might be consistent with assuming that, at 1-g_o, the angle of repose varied nearly linearly with rotation rate, (*i.e.*, $\theta_r \propto \omega^1$) as indicated by the DEM simulations described above (and consistent with measurements of Hill and Kakalios [22]). A reexamination of Klein and White's original video tapes revealed a minor systematic error that was overlooked in their original analysis. They intended for the flight tests to be run with a fixed rotation rate (*i.e.*, they did not intend to scale the rotation rate with the g-level); however, because the load on the drive motor varied with g-level there was a slight systematic variation of rotation rate with g-level in their tests. Figure 6 shows the variation of rotation rate with g-level found by analyzing videos of Klein and White's flight-tests with glass beads. The linear-fit curve shown in Figure 6 is,

$$RPM = 7.13 - 0.79(g/g_o), \tag{1}$$

where g/g_o is the g-level shown as the horizontal axis of the graph. This represents an approximately ±10% systematic bias on the nominal rotation rate of 6.75RPM, assumed by Klein and White in their analysis. The direction of this systematic bias is in the opposite direction of the shift in rotation-rate that our DEM simulations suggested would be desirable to maintain the same flow mode as the g-level varied. This is a relatively small systematic bias, nonetheless, a correction for this rotation-rate variation was incorporated in the reanalysis of Klein and White's data. Both the 1-g_o laboratory data (from Fig. 2 [25]) and the flight data (from Fig 1 [25]) of Klein and White were digitized and replotted; as the dynamic-angle-of-repose *vs.* the square root of (a_c/g), where a_c is the centrifugal acceleration at the periphery of the drum (due to its rotation), $a_c = R\omega^2$, where $R = 0.11m$, the radius of the drum, and ω is the drum rotation rate in radians per second, and g is the effective acceleration of gravity during the flight test in m/s^2. Figure 7 shows the replotted data from Klein and White's glass-bead tests [25]. The horizontal axis location for each flight data point has been adjusted by the linear-fit curve of Eqn (1), so that at lower g-levels, the slightly higher rotation rate is accounted for. Figure 7 is qualitatively very similar to Klein and White's Figure 2, with perhaps a slightly greater difference between trends in the flight-data and the lab-data, primarily because of the rotation corrections made in reanalyzing the flight-data. Conclusions that can be drawn from this revised analysis are qualitatively similar to those made by Klein and White. Also, as can be seen in Figure 7, the laboratory data (at 1-g_o) is consistent with a linear variation of angle-of-repose with rotation rate [Note, since $a_c = R\omega^2$, we find that $\sqrt{a_c/g} = \omega\sqrt{R/g}$, so that for a fixed radius and g-level, the scale of the horizontal axis of Figure 7 is proportional to the rotation rate of the drum, ω]. It should be noted that the video tapes of the KC-135 flight tests at the lowest g-levels showed a top-surface with some curvature. Thus, it is not entirely clear that the lowest g-level tests are still within the single-dynamic-angle-of-repose-regime. Nonetheless, it is also quite apparent that the entire set of flight data is not a simple extension of the 1-g_o laboratory data. The flight-data at various g-levels is clearly showing behavior that differs from the 1-g_o lab data.

The DEM simulations described above using purely cohesionless spheres, exhibited the same angle of repose over three orders of magnitude variation of g-level, as long as the drum rotation rate was scaled with the square root of the g-level. Clearly some phenomenon not included in the

cohesionless sphere simulations is affecting the flight-test material. As hypothesized by Klein and White, it might be that the 1.35*mm* diameter glass beads are showing the effects of interparticle cohesion (and/or a load-dependent interparticle friction coefficient [26]), and that one of the features of that interparticle interaction is a higher angle of repose at low *g*-levels. No cohesion or load-dependent friction was included in any of the DEM simulations.

A perhaps more significant feature of Klein and White's KC-135 tests, is the observation that the smooth glass beads exhibited a greater increase in angle of repose than did the angular sand particles. Both materials are comprised of particles of the same order of magnitude in size (~1.35*mm* and ~0.4*mm*) and their primary constituent is silica. It is likely that the larger change in angle of repose exhibited by the glass beads is because they were beginning to show the effects of interparticle cohesion as the gravity level was reduced as low as $0.1g_o$. We would expect to observe such effects with the glass beads before they would be seen with sand, as gravity is reduced, because the beads are relatively smooth spheres, and have relatively large-area 'spots' at the points where they contact each other, compared to the contacts of angular grains of sand [26]. The KC-135 tests may be indicating that a granular material comprised of ~1*mm* size particles can begin to exhibit some characteristics of a cohesive powder, e.g. a higher angle of repose, when the effective gravity acting on the material is reduced significantly.

When highly cohesive powders are placed in a slowly rotating drum, they do not usually flow easily, nor do they form a smooth top surface. Instead, cohesive powders build up large overhanging 'chunks' that can break off and collapse or cascade in random avalanches onto the material further down the slope. The time sequence for these large random avalanches is chaotic, and various powder-flow instruments have been developed based on evaluation of the time sequences of such flows [27-29]. Such instruments do not measure a fundamental property of the powder, such as its cohesive strength, but they can serve as a relative-index test to rank powders as to their ease of handling or 'flowability.' The glass beads and sand of Klein and White's tests did not exhibit behavior typical of highly cohesive powders; however the very fine, cohesive powders described in the remainder of this paper do not flow easily under 1-g_o laboratory conditions, and they would be expected to be even more problematic at lower *g*-levels.

2 Micro-Avalancher Observations of Cohesive Powder Flow

When a non-flowing, cohesive powder is placed in a rotating drum at elevated *g*-levels (*i.e.,* at the end of a centrifuge arm) the additional driving force of the elevated *g*-level can cause the powder to flow. If the *g*-level is elevated high enough, then the cohesive forces in the powder become completely overwhelmed by the elevated body forces, and the powder can flow like a typical cohesionless powder at 1-g_o. A series of cohesive powders were tested in a micro-avalancher consisting of a small rotating drum (either 3/8 inch diameter or ¼ inch diameter) and 1/8 inch thick (along the axis of rotation) located at the end of a centrifuge arm. The test cells were made of stainless steel, with glass covers on each end (sealed with O-rings outside of the test region, to

allow a controlled atmosphere or partial vacuum to be maintained inside the cell). The shape of the powder bed was illuminated by a strobe light synchronized with the centrifuge rotation so that a CCD camera could record the shape formed by the flowing powder bed. Under controlled humidity conditions (dry air with ~2%RH) and either atmospheric pressure or a partial vacuum, powders were tested at effective centrifuging *g*-levels ranging from a few g_o's to 1200 times terrestrial gravity. The rotation rate of the small drum was maintained at a fixed fraction of the rotation rate of the centrifuge arm in order to scale the drum rotation properly to produce self-similar flow conditions at all *g*-levels. The direction of rotation of the small cell was such that Coriolis forces acting on the powder flowing down the inclined slope tended to push the powder to the right in all photos shown. (When the small cell was rotated in the opposite direction the splash-zone at the bottom of the cell was usually larger than in the tests shown, and results were slightly less consistent).

Figure 8 shows representative changes in a cohesive powder's flow behavior in a drum that is slowly rotated while at the end of a centrifuge arm. Each column of pictures in Figure 8 represents a series of snapshots of the flowing powder at the same *g*-level, varying from $12.5g_o$ on the left to $400g_o$ on the right hand side. The powder shown in Figure 8 consisted of 20 to 70 micron lactose 'carrier' particles blended with 3.8wt% of a fine 1-micron size active pharmaceutical ingredient powder which was quite cohesive. The resulting powder was cohesive enough that at 1-g_o, the 42*mg* of powder in the cell did not move inside of the small drum (~ ¼" dia) when the drum rotated slowly. Once the *g*-level exceeded about $5g_o$ the powder began to move, and by $10g_o$ the behavior was quite consistent. The first column of snapshots on the left of Figure 6 is at a slightly higher *g*-level of $12.5g_o$. As can be seen in Figure 6, at $12.5g_o$ the powder behaved like a typical cohesive powder in a larger drum at 1-g_o; that is, it exhibited periodic avalanches when large chunks fell off at random time intervals. As the *g*-level increased to higher levels the powder behavior gradually changed to that of a free-flowing, or non-cohesive powder, exhibiting a smooth top surface with a single 'dynamic angle of repose.'

In addition to the change in flow behavior, the bulk density of the powder in the centrifuging drum tests also changed as the gravity level increased. The change in bulk density of the powder can be seen in Figure 8 by observing that the fraction of the area of the circle covered by powder in the snapshots is larger in the columns on the left hand side than in the columns on the right hand side. Because of this compaction at high *g*-levels, the flow characteristics of a powder can be different after being processed at each *g*-level. Powder removed after being processed at only $12.5g_o$ would be expected to have a lower yield strength and to flow more easily (at 1-g_o) than a powder that had been exposed to $400g_o$ body forces, and densification – collapsing some of the open structure existing because cohesive interparticle forces keep the powder from becoming a close-packed structure. Thus, a powder might flow better while at $400g_o$ than at $12.5g_o$, but, if it has been processed at $400g_o$ and then is brought back to terrestrial, or lunar, conditions, it may be compacted, and more difficult to remove from the processing container and/or to transfer to subsequent processing steps. This is one example of how the recent deformation and stress history

of a powder contributes to its flow behavior. Similar changes in angle of repose and density were observed for other powders tested.

Even very sticky, cohesive powders will flow if the *g*-level is raised high enough. Figure 9 shows the behavior of a powder comprised of only the micron-sized API powder which had been blended with the larger lactose particles for the powder samples of the previous figure. This powder was so cohesive that it stuck to the cell walls at effective gravity-levels below 100-g_o, and it was still exhibiting periodic avalanches at *g*-levels of 200 and 400, but behaved nearly like a free-flowing powder at 1200 g_o.

In the previously described DEM simulations (varying gravity from terrestrial level of 1-g_o up to 1000-g_o) the physical size of the simulated drum remained fixed (~137*mm* dia), and similar flows were obtained, as long as the rotation rate scaled with the square root of the effective gravity. In the micro-avalancher the physical size of the rotating drum (e.g., ~8*mm* dia) was much smaller than in the simulations, and it was observed that a smaller ratio of the centrifugal acceleration in the small drum to the effective *g*-level acting on it (e.g., $a_c/g_{eff} \sim 0.0001$) than had been used in the simulations (e.g. $a_c/g_{eff} \sim 0.01$) was needed in order to obtain flows with the same character (e.g., exhibiting a single-angle top surface). Previous physical tests with millimeter-scale sand and glass beads in rotating drums that were of a physical size comparable to the simulations (~137*mm* dia) had shown a single dynamic-angle-of-repose when the ratio of centrifugal acceleration in the drum to the effective *g*-level was around $a_c/g_{eff} \sim 0.01$ [31, 23]. This scaling of rotation parameters to obtain the same kind of flow in different sized drums, confirms the expectation that effects, like the duration of small avalanches, or inertial overshoot of the top surface, will vary with the physical size of the equipment.

3 Other Effects

The observations of granular flow in the KC-135 tests and in the micro-avalancher described in this paper were under either normal atmospheric pressure, or with a partial vacuum (~ 1 – 3 Torr). The micro-avalancher tests were performed under controlled humidity conditions (with less than 2%RH) in order to avoid crystallization of the amorphous raffinose powder. Also, in most of these tests, static-electric effects were small compared to the inertial and body forces acting on the granular materials involved. Such conditions are not likely to occur on the moon, at least not outside of human habitats. The hard vacuum of the lunar environment eliminates most adsorbed gases from surfaces, which results in higher effective surface energies, and therefore greater cohesive van der Waals forces acting between particles [34, 35]. It has, also, recently been recognized that most of the lunar surface is charged to a significant potential (of at least several volts) due to the UV photoelectric emissions on the sunlit side, and the solar wind bombardment on the dark side [36] (resulting in a net positive/negative surface charge on the lit/dark side, respectively). The net charge on the regolith particles, and the lack of a conductive *ground* to neutralize charges, will lead to substantial static-electric-charge effects. Both the increase in cohesion due to the higher surface energies, and the high static-charges will increase interparticle forces over those exhibited by the powders tested in this research. Thus, in addition to the effects

associated strictly with changes in the *g*-level, increased cohesion, and static charges will compound problems associated with powder flow in ISRU operations. Care needs to be taken to design ISRU equipment which can compensate for these incompletely understood effects.

4 Discussion and Conclusions:

Under lunar gravity the cohesive nature of powders will start to have an influence on the bulk deformation and flow properties of granular materials at much larger particle sizes than is typical of terrestrial powder flow operations. Several NASA studies of lunar and Martian dust have examined tribo-electrification and potential charge buildup on equipment and particle surfaces and subsequent adhesion due to static charge effects. Often overlooked in these studies, however, is the fact that all materials (whether they have a net surface charge or not) exhibit surface energy forces, that are very short range, but come into play once surfaces are 'touching.' These van der Waals forces are due to the dispersive and polar surface energies inherent at material boundaries. Terrestrially, dry powders with mass-median particle sizes larger than around 100 to 200μm, seldom exhibit strong 'cohesive' powder behavior, and such powders are usually described as 'free flowing.' As particle size decreases, however, the amount of surface area per unit mass increases, and surface-energy forces have a greater influence on bulk powder flow characteristics. For contacting particles that are smaller than ~10μm, such forces can be strong enough to cause plastic deformation on particle surfaces near the points of contact – even with no applied external loads [32]. The bulk behavior of such fine powders can be dominated by their *cohesiveness*. The exact particle size at which plastic deformation might be expected to become significant depends on the surface energy, elastic modulus, and yield strength of the particles involved [33, 37]. The large proportion of very fine particulates in typical regolith, combined with reduced gravity and potentially reactive surface chemistry, will contribute to physical characteristics which are apt to differ substantially from those exhibited by material in typical terrestrial resource recovery processes.

Body forces due to gravity, and thus lithostatic loads, are reduced by about a factor of six on the moon. Inertial forces required to accelerate or centrifuge masses are, however, still the same as terrestrially. Most terrestrial mineral processes utilize gravity to initiate flow into feeders, onto conveyors, or out of buckets or hoppers. For the same size equipment, the body force per unit area, at equipment openings, on the moon will be reduced by a factor about equal to the reduction in gravity (*i.e.*, by about a factor of six) over what is typical on earth. In order to initiate flow, due solely to lunar gravity, the size of equipment openings will need to be scaled to larger dimensions. In order to obtain flow conditions similar to those achieved terrestrially, this may require increases in equipment-opening sizes as great as a factor of 6, in some cases; in other cases, it may require less of an increase in equipment-opening dimensions. If lunar resource transport and handling equipment openings are not scaled to larger sizes than is typical for terrestrial designs, then it will

probably be necessary to utilize alternative means of initiating and/or maintaining flow into, out-of, or within various processing stages, such as pneumatic, vibration, or centrifugal forces.

Changes in *g*-level by a factor of 4, (e.g., going from $25g_o$ to $100g_o$ in Figure 8) changed the behavior of cohesive API/Lactose blended powders, from random large avalanches, to that of a typical non-cohesive powder, exhibiting a smooth flowing top surface with a single dynamic angle of repose. A factor of four change in *g*-level caused similar changes in avalanching $4\mu m$ BCR-Limestone powder [30], going from $165g_o$ to $660g_o$, in a slowly rotated 3/8-inch diameter drum.

There are a variety of reasons to expect powders made from lunar regolith to be cohesive. First, decreasing particle size increases cohesion relative to other forces acting on particles in a powder, and lunar regolith contains a very significant fraction of very fine particulates. Second, the lack of humidity and an atmosphere has left the surfaces more chemically reactive than typical terrestrial materials, thus the surface energy is likely higher than is typical in mineral processing operations terrestrially. Third, the lack of an atmosphere eliminates aerodynamic drag forces which are a major factor acting on particles in powders terrestrially (Elimination of aerodynamic forces may allow the effects of interparticle cohesion to be more apparent than would be the case if aerodynamic forces overwhelmed interparticle cohesion). Fourth, the lunar surface is likely charged to several volts, and thus, regolith particles will have a net charge, and exhibit static-electric interactions with each other and with other surfaces. Finally, and the primary subject of the study described in this paper, decreasing gravity decreases the major driving force acting on materials in many processing operations, thus causing assemblies of particles (*i.e.*, powders) to appear to be more cohesive in their bulk behavior than they would on earth.

Acknowledgments

Most of the powder measurements and simulations described in this paper were made by the authors when they were employees of Inhale Therapeutic Systems (now Nektar Therapeutics) San Carlos, CA. Preparation of this paper was partially supported by NASA through contract NNM05AA88C, and through contract NNC06VC87P technically supervised by Allen Wilkinson, Glenn Research Center. NASA's support is gratefully acknowledged. The helpful suggestions of the referees are, also, much appreciated.

References

1. Carrier III, W.D., G.R. Olhoeft, and W. Mendell "Chapter9: Physical Properties of the Lunar Surface," in *Lunar Sourcebook: a User's Guide to the Moon*, G.H. Heiken, D.T. Vaniman, and B.M. French, editors, Cambridge University Press, 1991(available on CD as LPI Contribution No. 1259, Lunar and Planetary Institute)
2. Todd, P. "FINAL PROGRESS REPORT on ROBOTIC LUNAR ECOPOIESIS TEST BED," for NASA-NAIC-USRA, Prime Contract NAS5-03110, Research Subcontract 07605-003-020, Space Hardware Optimization Technology, Inc., Greenville, Indiana, 30 April, 2004.

3. Taylor, L.A., H.H. Schmitt, W.D. Carrier III, M. Nakagawa "The Lunar Dust Problem: From Liability to Asset," *AIAA, 1st Space Exploration Mission*, Jan., 17, 2005

4. Schwedes, J., *Granular Matter* **5**, 1 (2003); also, Schwedes J. "Measurement of flow properties of bulk solids," *Powder Technology*, Vol **88**, No. 3 (1996) pp285-290.

5. Prescott, JK, and RA Barnum, "On Powder Flowability," *Pharmaceutical Technology*, Oct 2000, p60.

6 Jenike, A.W., *Storage and flow of solids, Bulletin 123,* Engineering Experiment Station, University of Utah, 1964.

7. Schulze, D. and A. Whittmaier, *Chem. Eng. Technol.* **26**, 2, (2003).

8. Svarovsky, L., *Powder Testing Guide: Methods of Measuring the Physical Properties of Bulk Powders*, Elsevier Applied Science, England 1987.

9. Castellanos, A. , J.M. Valverde, and M.A.S. Quintanilla, " The Sevilla Powder Tester: A tool for Characterizing the Physical Properties of Fine Cohesive Powders at Very Small Consolidations," *Kona* No **22** (2004) p66-80.

10. Carr, R.L., "Evaluating flow properties of solids," *Chem Engng*. **18** (1965) p163-168.

11. [the time that a given mass of powder takes to discharge through a hopper] *Book of ASTM Standards, Part 9,* American Society for Testing and Materials, Philadelphia, 45, 1978.

12. Hausner, H.H., *Int. J. Powder Metallurgy*, **3**(4), (1967) 7.

13. Abdullah and Geldart, *Powder Technol*.**102** (1999) 151-165.

14. Walton,O.R., C.P. De Moor, D.P. Miller, "Simulation of Low-Stress Compaction of Cohesive Micron-Scale Powders," AIChE 2003 Annual Meeting, Nov. 16-21 (2003) (Session T4-35a), San Francisco, CA.

15. Miller, D.P., D. Lechuga-Ballesteros, L. Williams, T. Tan, J. Kanda, W. Foss, O. Walton, A. Mandel, and X. Cai (2002) "Dispersibility of Spray- dried Raffinose: Effects of Particle Size and Relative Humidity," AAPS Annual Meeting –Nov. 10-14, 2002 - Toronto, Canada.

16. Brown RL, and JC Richards, *Principles of Powder Mechanics*, Pergamon Press, Oxford, 1970.

17. Walton, O. and K. Gill "Simulation of Rotating Drum Flows – an Assessment of Sensitivity to Discrete Particle Modeling Parameters," AIChE Particle Technology Forum, Reno, NV, Nov 4-9, 2001, (Session 03A01)

18. Walton, O.R., "Numerical Simulation of inclined Chute Flows of Monodisperse, inelastic, Frictional Spheres," *Mech. of Materials*, **16** (1993) p239-247.

19. Hanes, D.M., and O.R. Walton "Simulations and physical measurements of glass spheres flowing down a bumpy incline," *Powder Technology*, **109** (2000) 133-144.

20. Walton, O.R., and R.L. Braun "Viscosity and Temperature Calculations for Assemblies of inelastic Frictional Disks," *J. Rheology*, **30**(5), (1986) 949-980.

21. Jaeger, H.M., J.B. Knight, C. Liu, and S.R. Nagel "What is Shaking in the Sandbox?" *Materials Research Soc. Bul*., **19**(5) (1994) p25-31.

22. Hill , K.M., and J. Kakalios "Reversible axial segregation of rotating granular media**,"** *Phys. Rev. E*, Vol. **52**, No. 4 (1995) p4393-4400.

23. Walton, O.R., and R.L. Braun "Simulation of Rotary-Drum and Repose Tests for Frictional Spheres and Rigid Sphere Clusters," Joint DOE/NSF Workshop on Flow of Particulates and Fluids, Sept 29- Oct 1, (1993) Ithaca, NY. (paper available at: www.grainflow.com).

24. Walton, O.R. "Centrifuged Rotating Drum for Treating Cohesive Powders," US Patent Application Publication No.: US 2003/0003229A1, Pub. Date: Jan. 2, 2003.

25. Klein, S. P., and B. R. White "Dynamic shear of granular material under variable gravity conditions," AIAA Ann., 88– 0648 (1988).

26. Tüzün, U., M.J. Adams, and B.J. Briscoe "The Theoretical Prediction of the Effects of Particulate Properties on the Wall Friction Angles Measured for Smooth Silo Walls," *Proceedings of the 2nd International Conference on Bulk Materials Storage, Handling and Transportation*, Wollongong University, A.W. Roberts, editor, The Institute of Engineers, Australia, July 5-11, 1986.

27. Kaye, B. H. (1997) "Characterizing the flow of metal and ceramic powders using the concepts of fractal geometry and chaos theory to interpret the avalanching behavior of a powder," In T. P. Battle and H. Henein (eds.), *Processing and Handling of Powders and Dusts*, Minerals Metals & Materials Society, Warrendale, PA, 1997 pp. 277–282.

28. Lavoie, F., L. Cartilier, and R. Thibert (2002) "New Methods Characterizing Avalanche Behavior to Determine Powder Flow", *Pharmaceutical Research,* Vol. **19**, No. 6, p887-893, June 2002

29. Valverde, J., A. Castellanos, A. Ramos (2000) **"**Avalanches in fine, cohesive powders," *Phys. Rev. E*, **62**(5) p6951.

30. Institute for Reference Materials and Measurements Directorate General Joint Research Centre of the European Commission.

31. Pitts, J.H., and O.R. Walton "Granular Flow Along the Interior surface of Rotating Cones,", Proceeding 8th Int. CHISA Mtg., Prague, Czechoslovakia, September 3—7, 1984 (also available as LLNL report UCRL-90742 Preprint); and Pitts, J.H., O.R. Walton and R.L. Creedon "A High-Temperature, Low-Activation Design for the Cascade Reactor," *Transactions of the Am. Nuclear Soc.,* Vol. 46, pp. 247-248 (1984).

32. Rimai, D.S., and D.J. Quesnel, *Fundamentals of Particle Adhesion* (2001) Polymer Surfaces and Interfaces Series, M.W. Urban, Ed., Global Press, ISBN 1-890086-04-5.

33. Walton, O.R.(2004) "Potential discrete element simulation applications ranging from airborne fines to pellet beds," *SAE 2004 Transactions J. Aerospace* paper 2004-01-2329, p471 (paper available at: www.grainflow.com).

34. Lee, L-H., "Adhesion and cohesion mechanisms of lunar dust on the moon's surface," *Fundamentals of Adhesion and Interfaces*, Rimai, DeMejo and Mittal (Eds.), VSP, (1995) p73-94.

35. Salisbury, J.W, P.E. Glaser, B.A. Stein and B Vonnegut, “Adhesive Behavior of Silicate Powders in Ultrahigh Vacuum,” *J. Geophys. Res*. **69**, 235 (1964).

36. Sickafoose, A.A, J.E. Colwell, M. Horanyi, and S. Robertson, “Experimental levitation of dust grains in a plasma sheath,” *J. Geophs. Res*. **107** (A11), 1408 (2002).

37. Maugis, D., and H.M. Pollock “Surface forces, deformation and adherence at metal microcontacts,” *Acta Metall*. Vol. 32, No. 9, (1984) pp1323-1334.

Figure Legends:

Figure 1. Uniaxial compaction of cohesive powders comprised of lunar regolith [1] and spray-dried, amorphous raffinose [14, 15]. The horizontal portion at the left end of each curve is likely reloading to conditions under which the sample was prepared [any unloading-reloading would occur along nearly horizontal lines branching to the left off of each curve]. The knee to less compressible behavior at high pressure probably indicates a change in the mode of deformation (*i.e.*, possibly changing from collapse of an initially 'open' structure by particle rearrangement, to a more-usual compact configuration where further compaction occurs by much smaller-scale particle rearrangement, or by particle deformation or damage). Compaction has nearly ceased by 1-Bar load for the regolith, but would be expected to resume at higher loadings as porous particles fracture and crush.

Figure 2, Amorphous raffinose powder spray dried from aqueous solution (1 wt% solids content) in a modified Büchi spray dryer [15]

.

Figure 3 DEM Simulation of cohesionless, frictional spheres in a partially filled, slowly rotating drum [17]

Figure 4 (a) and (b) Simulated flow of cohesionless spheres in a rotating drum with $a_c = 1.0g_{eff}$ [23]; (c) $4\mu m$ BCR-Limestone powder [30] in a 3/8" diameter rotating drum in a planetary-mill configuration with $a_c = 0.8g_{eff}$, when $g_{eff} = 330g_{terrestrial}$ [24].

Figure 5 Schematic of a planetary-mill configuration with two matching planetary rotating drums (one at each end of a centrifuging arm). The effective *g*-level, g_{eff}, is taken to be the centrifugal acceleration at the center of rotation of the small drums, $A_c = R_1\Omega_1^2$, where Ω_1 is the rotation rate of the main centrifuging arm, and R_1 is the distance from the center of the centrifuge to the center of either of the small drums. The extra centrifugal acceleration at the periphery of either small drum due to its separate rotation is $a_c = r_c\Delta\omega^2$, where $\Delta\omega$ is the rotation rate of the small drum with respect to the rotation of the centrifuge, and r_c is the inner radius of the small drum.

Figure 6 Variation of rotation rate with *g*-level in Klein & White's flight-tests of glass beads in a partially filled rotating drum [25] (obtained from analysis of original flight-test videos).

Figure 7 Dynamic Angle of Repose for glass beads in a rotating drum at various *g*-levels from 0.1 to $1.8g_o$ at a nominal rotation rate of ~6.75RPM, and for the same material at 1-g_o in the laboratory at various rotation rates [25].

Figure 8. Snapshots of a $42mg$ powder sample, comprised of (20-70μm) lactose particles blended with fine particles (~1μm) of a cohesive active pharmaceutical ingredient (API) in a slowly rotating cell, in a small planetary-mill configuration, with the centrifugal acceleration on the periphery of the cell, a_c, maintained at a fixed fraction of the main centrifuging acceleration, A_c, ($a_c/A_c = 0.0001$).

Figure 9. Snapshots of a very fine (~1μm) and very cohesive active pharmaceutical ingredient (API) powder in a slowly rotating micro-avalancher at effective gravity levels from 12.5 to 1200.

Figure 1

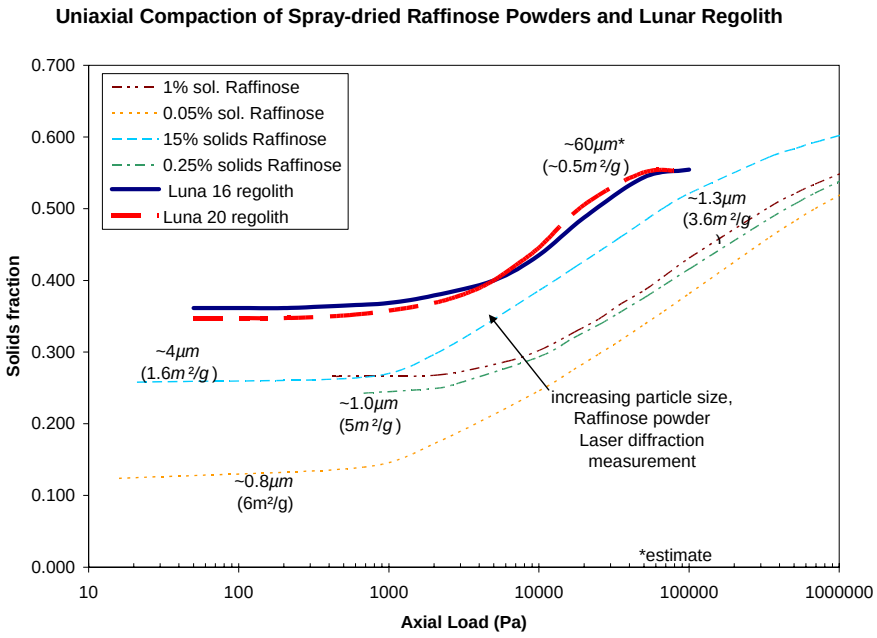

Figure 2

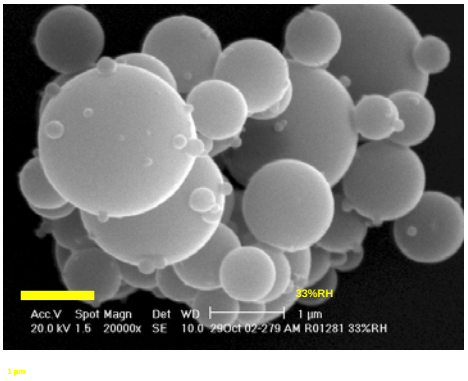

Figure 3

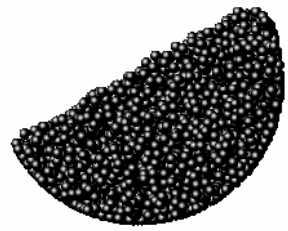

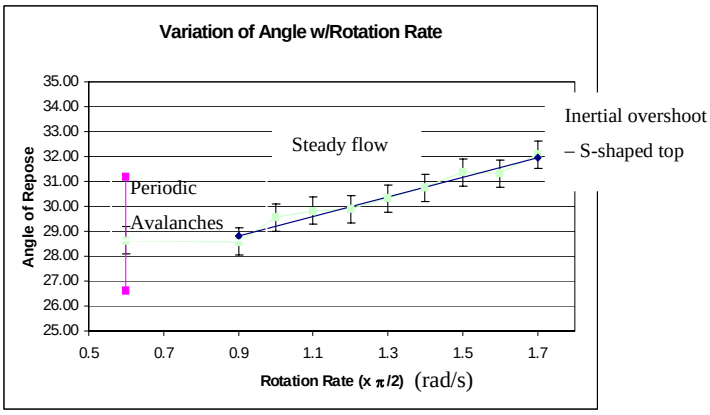

Figure 4

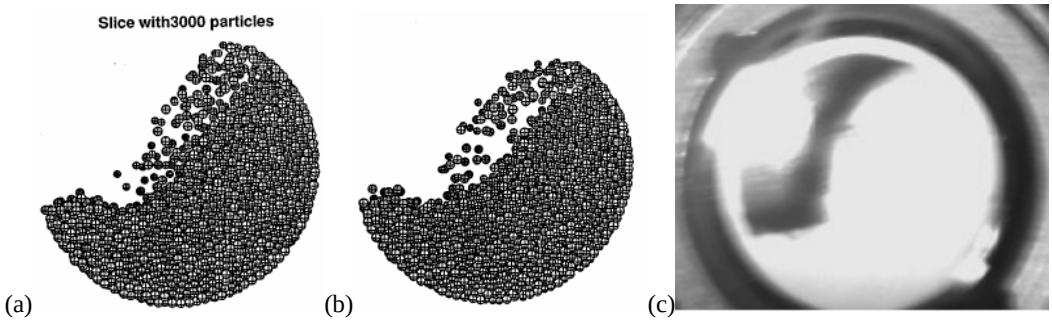

Figure 5

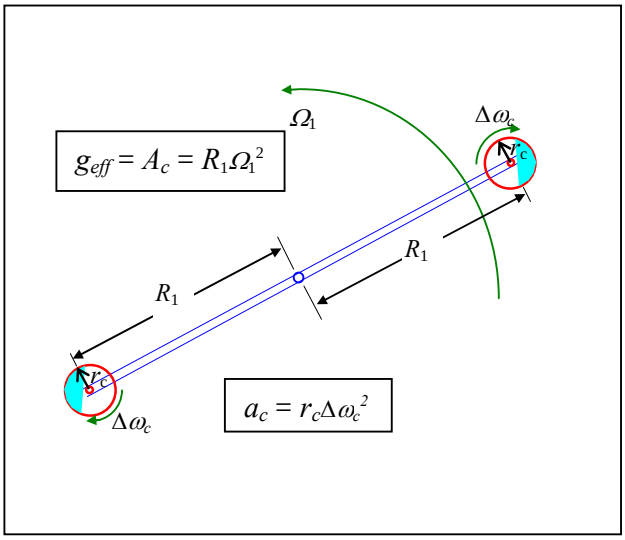

Figure 6

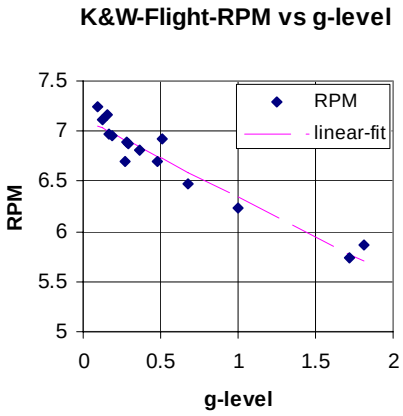

Figure 7

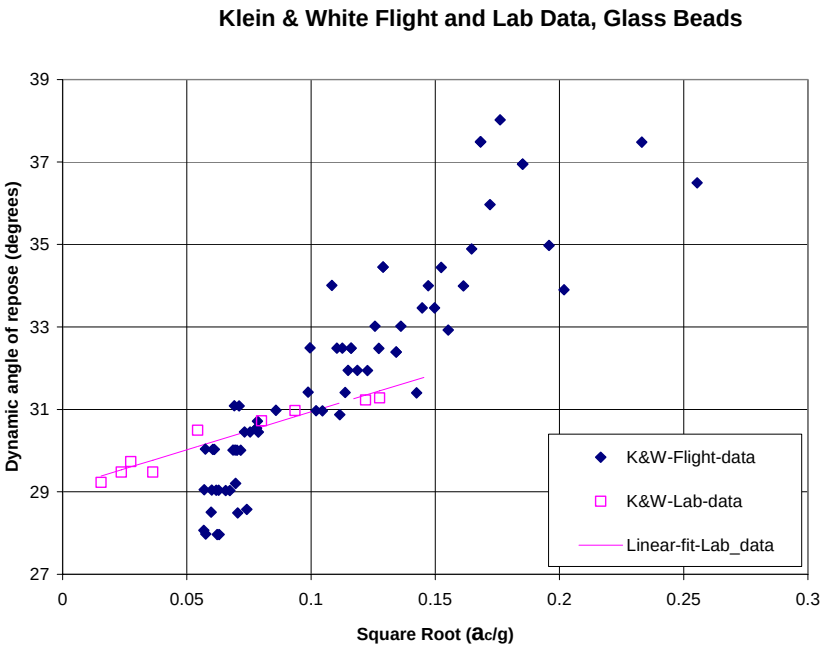

Figure 8

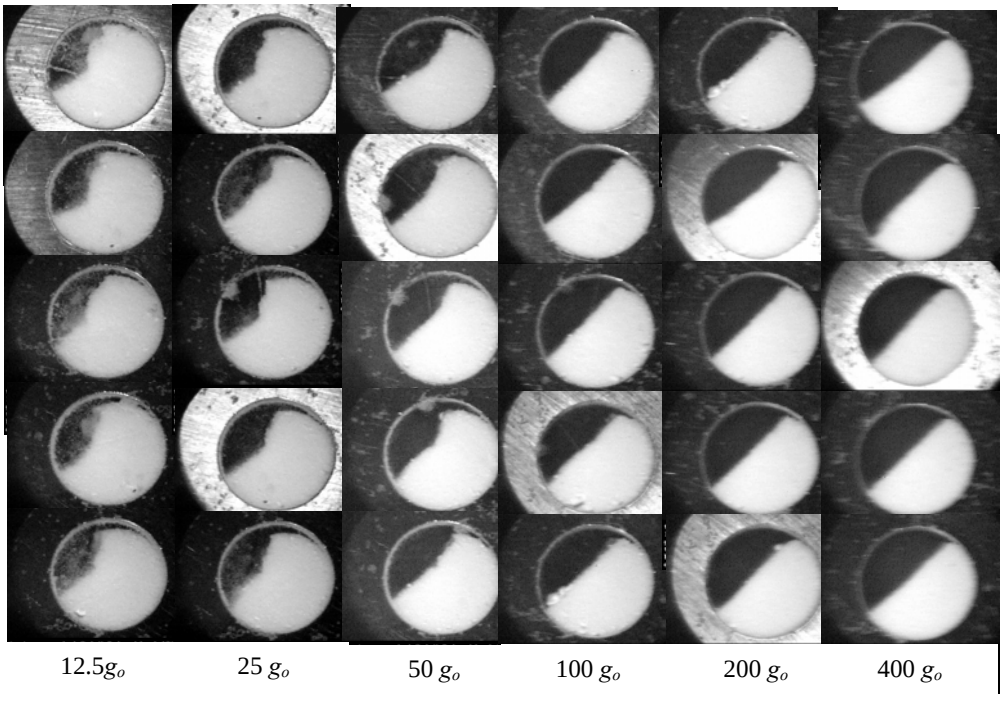

Figure 9

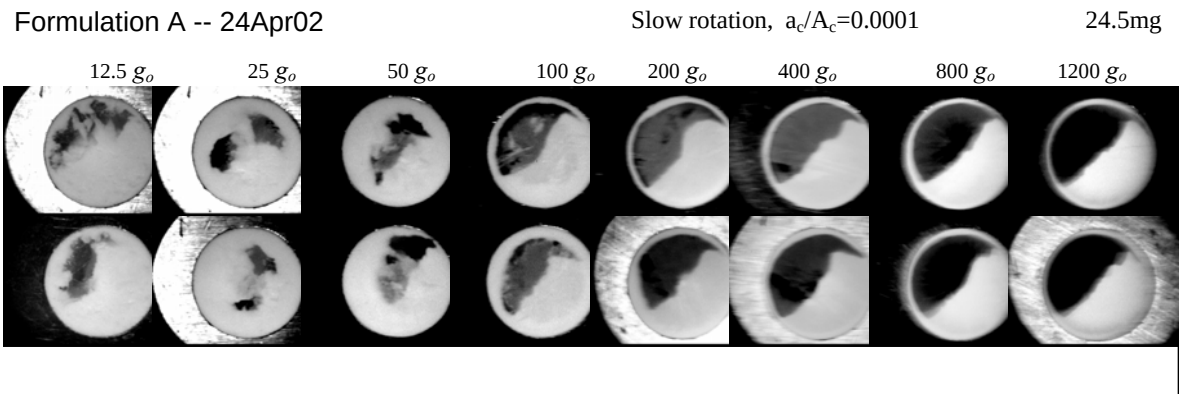
Formulation A -- 24Apr02
Slow rotation, a_c/A_c=0.0001
24.5mg
12.5 g_o
25 g_o
50 g_o
100 g_o
200 g_o
400 g_o
800 g_o
1200 g_o